HELIOS Benchmark Calculation:
Radiation-Driven Capsule Implosion in Z-Pinch Dynamic Hohlraum

In this *HELIOS* benchmark simulation, a spherical capsule embedded in a low-density CH_2 foam is imploded by an external radiation field. The parameters utilized in this benchmark simulation are taken from z-pinch-driven dynamic hohlraum experiments performed at the Z facility at Sandia National Laboratories [1]. The time-dependent hohlraum radiation field is constrained by on-axis XRD and bolometer measurements. The trajectory of the capsule implosion is obtained from x-ray framing camera measurements. We compare the simulated capsule implosion trajectory with experimental data.

Schematic illustrations of the original z-pinch dynamic hohlraum and capsule configurations are shown in Figures 1 and 2. The tungsten wire array implodes onto a cylindrical CH_2 foam. The tungsten impacts the foam, heating the tungsten and sending a shock into the foam. Radiation from the tungsten fills the foam, and the radiation heats and ablates the outer layer of the capsule, driving the implosion.

Figure 1. Illustration of capsule embedded in CH_2 foam in z-pinch-driven capsule implosion experiment.

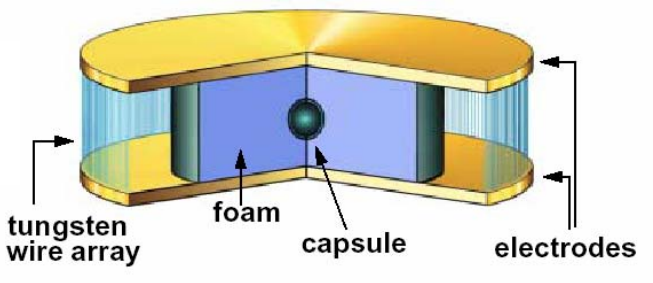

The embedded spherical capsule is a 2.1 mm-diameter CH capsule with a 55.3 μm-thick wall. The CH is coated with 4.5 μm of PVA (C_2H_4O). The capsule is filled Ar-doped DD with 12 atm DD and 0.075 atm Ar. While the 5 mg/cm^3 CH_2 foam is cylindrical in the experiment, it is modeled as a spherical shell in our 1-D *HELIOS* simulation. The assumption is that as the foam heats up it becomes optically thin, so that the top and bottom of the capsule (the poles) see approximately the same radiation field as the capsule side (the equator).

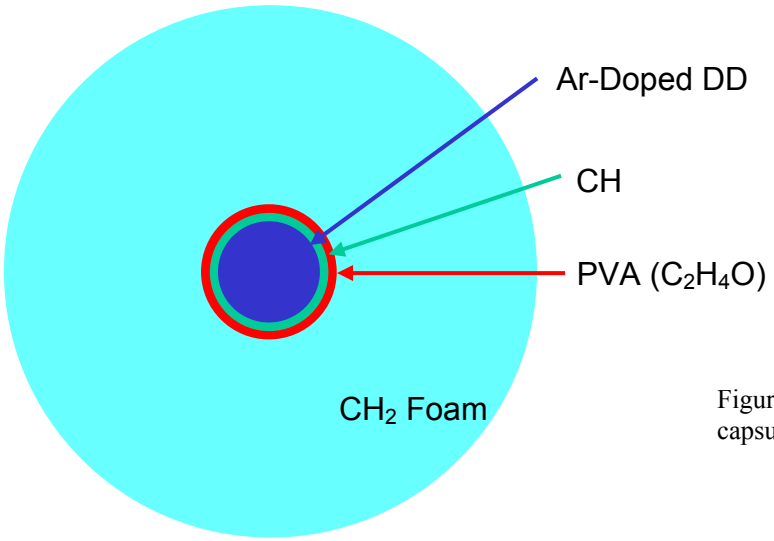

Figure 2. Illustration of foam-embedded capsule.

SESAME [2] equations of state were used for all materials in this simulation. Multigroup opacity data were obtained from *PROPACEOS* calculations. (*PROPACEOS* is a code used to generate multigroup opacity and equation of state data based on *ATBASE* atomic data [3] and physics modules in the *SPECT3D* Imaging and Spectral Analysis package [4].) For each material, the appropriate atomic composition was used for the multigroup opacities. Radiation transport was computed using the flux-limited diffusion model and 100 frequency groups.

The radiation drive is shown in Figure 3. The external drive applied to the outer boundary of the CH_2 foam is specified by a time-dependent radiation temperature. At each point in time the external source is assumed to have a Planckian spectral distribution. The duration from the start of the *HELIOS* simulation ($t = 0$ ns) to the peak in the radiation flux is 100 ns. The drive at $t > 84$ ns is based on XRD and bolometer radiation flux measurements from the Z experiments. At earlier times, a relatively low-temperature foot is applied, which is estimated from side-on (*i.e.* off-axis) XRD/bolometer measurements from earlier experiments. This is used because the radiation does not heat the interior of the foam until approximately this time, and therefore the foam interior – which is viewed by the on-axis XRD/bolometer diagnostics – does not have a radiation temperature that is indicative of the radiation field at the outer boundary of the foam.

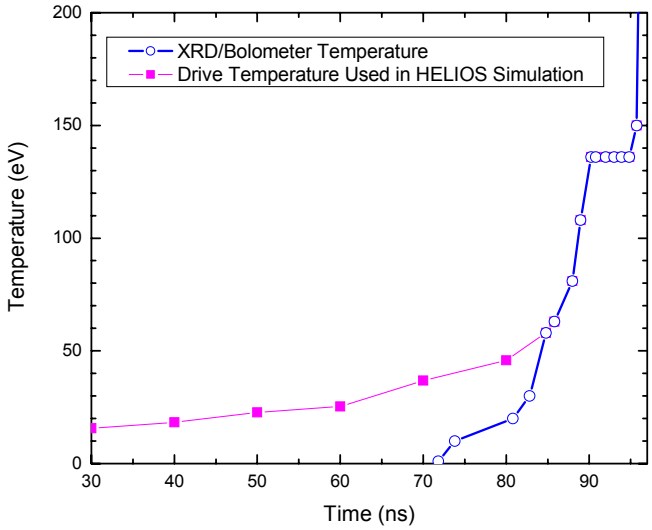

Figure 3. Time-dependent external radiation drive used for z-pinch-radiation-driven capsule implosion simulation.

Results

Figure 4 shows the Lagrangian zone positions as a function of time. The different color curves represent the different materials in the simulation. The experimental data is represented by the magenta squares. The agreement between the simulation and experimental shock breakout data is seen to be very good, as the simulated capsule compression follows the measured radius throughout the implosion.

Figure 5 shows the temperature distribution in the capsule and foam at simulation times ranging from 70 to 95 ns. It is seen that by 85 ns, the radiation has burned through the foam to the capsule surface (located at $r = 0.1$ cm). For comparison, the radius of the diagnostic hole for the on-axis diagnostics ($R_{max} = 0.25$ cm) is also shown.

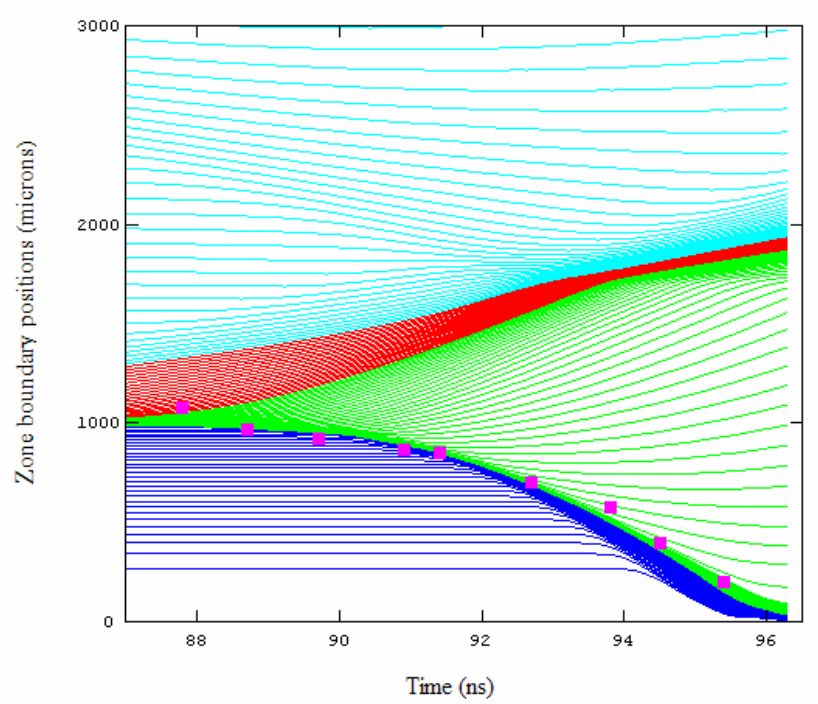

Figure 4. Comparison between Lagrangian zone positions from *HELIOS* simulation and experimental measurements of capsule radius (magenta symbols). Blue: Ar-doped DD; green: CH ablator; red: PVA; cyan: CH_2 foam.

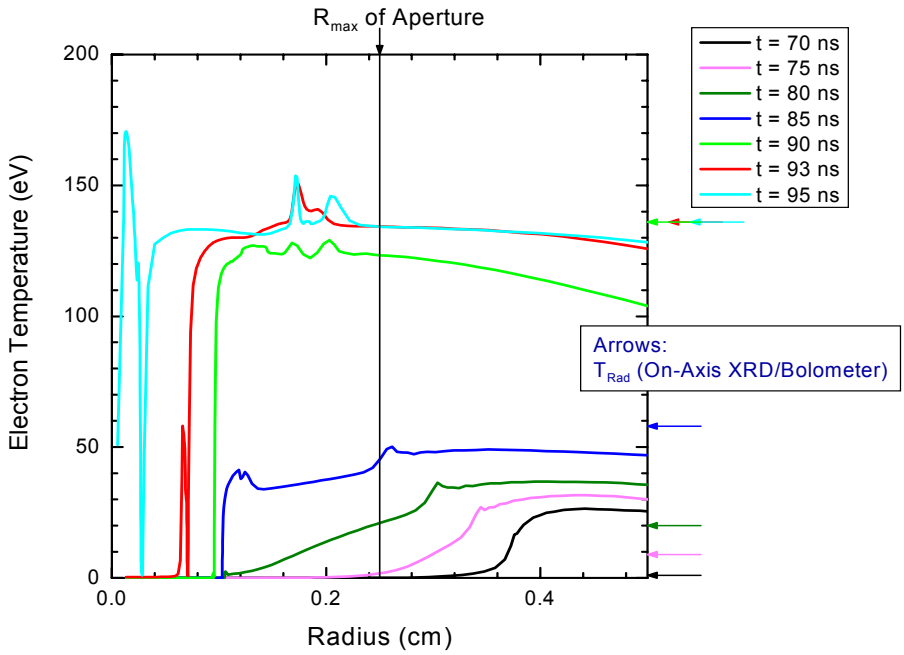

Figure 5. Temperature distributions from *HELIOS* simulation of radiation-driven capsule implosion.

As a further test of the *HELIOS* radiation-hydrodynamics simulation, the *HELIOS* results are post-processed using *SPECT3D* in order to compare spatial intensity distributions with x-ray framing camera data. Figure 6 shows images computed using *SPECT3D* at simulation times of t = 89.4 ns and 91.2 ns. Results are shown for photon energy cuts at $h\nu$ = 250 eV (top images) and $h\nu$ = 500 eV (bottom images). In each of the images, brighter emission is observed at the radius of the ablator. This is consistent with the experimental framing camera data that shows "limb brightening" about the capsule at a location consistent with the ablation plasma [1].

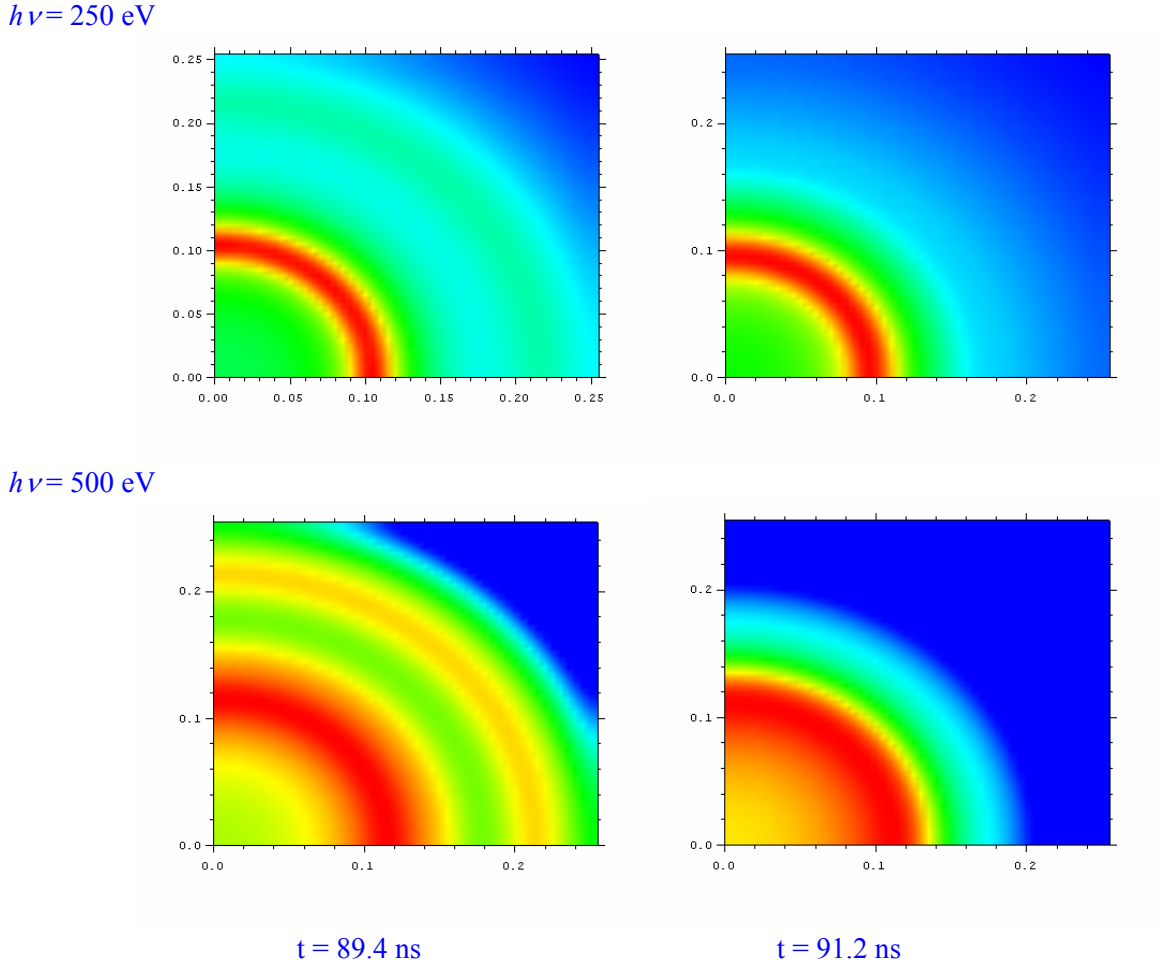

Figure 6. Color contour images of intensities obtained using post-processed temperature and density distributions from *HELIOS* at simulation times of t = 89.4 (left) and 91.2 ns (right). Results are shown for intensities computed at $h\nu$ = 250 eV (top) and $h\nu$ = 500 eV (bottom). Intensity color scales vary for each image. The calculated images include the effects of the 200 μm spatial resolution for framing camera.

More quantitative comparisons with the framing camera data are shown in Figures 7 and 8. Figure 7 shows lineouts of the simulated framing camera images calculated at simulation times from 87.6 ns to 92.6 ns. The plot on the left shows lineouts for the *frequency-integrated* intensity, while the plot on the right shows intensity lineouts for a photon energy of $h\nu = 250$ eV. In each case the intensity profiles are normalized to the intensity at $r = 0$ (*i.e.*, a line of sight that goes through the center of the capsule).

Note that while both the frequency-integrated lineouts and the $h\nu = 250$ eV lineouts show limb brightening at a radius of ~ 0.1 cm, the contrast is significantly greater for the $h\nu = 250$ eV lineouts. This is due to the fact that carbon exhibits relatively little absorption (and emission) below its K-edge. For the frequency-integrated case, the ablation region exhibits ~ a few tens of percent greater emission at the limb that at the capsule core, while in case of the $h\nu = 250$ eV lineouts the limb-to-core contrast is ~ 2.0 – 2.7.

Figure 8 compares the calculated $h\nu = 250$ eV lineout at $t = 87.6$ ns (solid curve) with the lineout from the experimental kimfol-filtered x-ray framing camera data. The kimfol framing camera data is dominated mainly by 250 eV photons [1]. The calculated intensity profiles and kimfol data are seen to be in good general agreement, as the limb-to-core intensities are both predicted to be ~ a factor of 2.2 – 2.5.

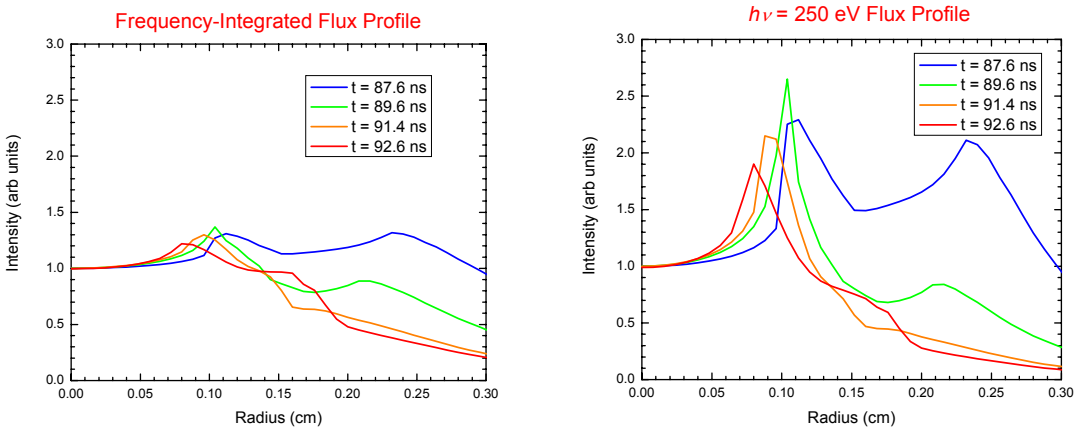

Figure 7. Calculated intensity profiles from simulated framing camera images obtained by post-processing of *HELIOS* capsule implosion simulations. Left: frequency-integrated lineouts. Right: intensity lineouts at $h\nu = 250$ eV. The radius of $r = 0$ corresponds to a line-of-sight going through the center of the capsule.

Figure 8. Comparison of calculated intensity profile at $h\nu = 250$ eV and $t = 87.6$ ns (solid curve) with experimental kimfol-filtered framing camera data (dashed curve). The calculated profile includes the effects of the 200 μm spatial resolution for framing camera.

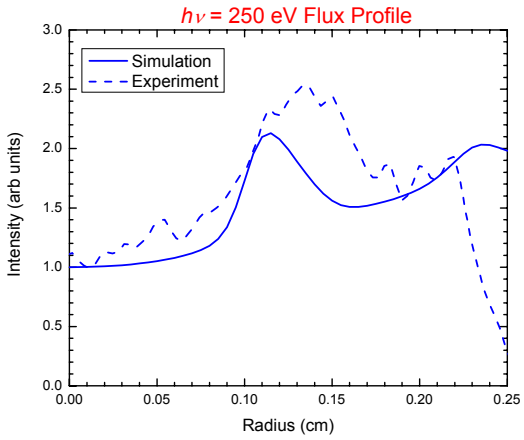

The above benchmark case shows that the *HELIOS* simulation, which utilizes a radiation drive history based on experimental XRD/bolometer measurements, predicts the evolution of the capsule implosion accurately. In addition, the post-processed temperature and density profiles from the *HELIOS* simulation produce emergent intensity distributions that are in good agreement with kimfol-filtered x-ray framing camera measurements.

References

[1] J. E. Bailey, *et al*., Phys. Rev. Lett. **89**, 095004 (2002).

[2] "SESAME: The Los Alamos National Laboratory Equation of State Database," LANL Report No. LA-UR-92-3407, edited by S. P. Lyon and J. D. Johnson (1992).

[3] P. Wang, "*ATBASE User's Guide*," University of Wisconsin Fusion Technology Institute Report No. UWFDM-942 (1993).

[4] J. J. MacFarlane, *et al*., "*SPECT3D Imaging and Spectral Analysis Suite*," Prism Computational Sciences Report No. PCS-R-037 (2003).